doi.org/10.36721/PJPS.2026.39.11.302.1

Molecular mechanism of ephedrine-regulated ferroptosis in asthma via PKM2–ACSL4 lactylation

Lanting Zhao*, Rong Xia, Shuang Zeng and XiaoXia Yan
Department of Respiratory Medicine, Lanzhou University Second Hospital, Lanzhou, Gansu, 730030, China

Abstract: **Background**: Asthma is a chronic airway inflammatory disease with limited curative options. Ephedrine (EP), a natural alkaloid, has shown anti-asthmatic effects, but its molecular mechanism remains incompletely understood. Ferroptosis, an iron-dependent lipid peroxidation cell death pathway, aggravates airway epithelial injury in asthma. Pyruvate kinase M2 (PKM2) generates lactate, which can drive protein lactylation; however, whether EP acts by modulating PKM2-dependent lactylation of acyl-CoA synthetase long-chain family member 4 (ACSL4) to inhibit ferroptosis is unknown. **Objectives**: To investigated whether EP attenuates ferroptosis-driven asthmatic progression by suppressing PKM2-dependent lactylation of ACSL4. **Methods**: LPS-stimulated BEAS-2B cells and ovalbumin (OVA)-sensitized rats were used as in-vitro and in-vivo asthma models, respectively. Cell proliferation (CCK-8), apoptosis (TUNEL), inflammatory cytokines (ELISA) and oxidative/lipid peroxidation markers (ROS, Fe^{2+}, MDA, LPO, SOD) were measured. PKM2 and ACSL4 expression were determined by qPCR and Western blot; ACSL4 lactylation was assessed by co-immunoprecipitation. *In-vivo*, asthma behavioral scores, airway resistance (RL), dynamic compliance (Cdyn), lung histology (HE) and bronchoalveolar lavage fluid cytokines were evaluated. **Results**: *In-vitro*, EP restored cell viability, reduced apoptosis and cytokine release and inhibited ferroptosis ($P < 0.05$). LPS upregulated PKM2; EP reversed this, whereas PKM2 overexpression abolished EP's protection ($P < 0.05$). PKM2 overexpression increased ACSL4 transcription and lactylation, effects attenuated by EP. Silencing ACSL4 reversed PKM2 overexpression-induced injury and ferroptosis ($P < 0.05$). *In-vivo*, EP alleviated OVA-induced asthmatic symptoms and pulmonary pathological changes. **Conclusion**: EP mitigates asthma by down-regulating PKM2, thereby blocking ACSL4 lactylation and ferroptosis-mediated airway epithelial injury. The PKM2-ACSL4 lactylation axis represents a novel therapeutic target.

Keywords: Asthma; Ephedrine; Ferroptosis; Lactylation; PKM2

Submitted on 21-12-2025 – Revised on 10-04-2026 – Accepted on 13-04-2026

INTRODUCTION

Bronchial asthma is a chronic airway inflammatory disease characterized by hyper-responsiveness, reversible airflow limitation and episodic respiratory symptoms (Lommatzsch *et al*., 2023; Melen *et al*., 2024). Current therapies, including bronchodilators and glucocorticoids, control symptoms but cannot cure the disease and the need for novel mechanism-based treatments remains (Nguyen and Nasir, 2024; Yasaratne *et al*., 2023). Ephedrine (EP), a natural alkaloid from Ephedra species, is clinically used as a bronchodilator (Gad *et al*., 2021). Beyond its bronchodilator activity, accumulating evidence indicates that EP exerts broad anti-inflammatory effects in cerebral ischemia-reperfusion injury, chronic obstructive pulmonary disease, ischemic stroke and pulmonary fibrosis (Shi *et al*., 2021; Wang *et al*., 2022; Huang *et al*., 2021; Tian *et al*., 2023). Moreover, EP has been shown to attenuate airway inflammation and restore Th1/Th2 balance in murine asthma models (Hu *et al*., 2024). Nevertheless, the precise molecular mechanisms through which EP confers protection in asthma remain incompletely understood.

Pyruvate kinase M2 (PKM2) is a glycolytic enzyme that is upregulated in asthmatic airways and promotes M1 macrophage polarization and aberrant glycolysis, contributing to airway inflammation (Yang and Lu, 2015, van de Wetering *et al*., 2021). Notably, PKM2 activity generates lactate, which can drive a recently identified post-translational modification called protein lactylation, in which lactyl groups are covalently added to target proteins. Lactylation modulates gene expression and protein function and has been implicated in inflammation and ferroptosis (Jing *et al*., 2025).

Acyl-CoA synthetase long-chain family member 4 (ACSL4) is a key executor of ferroptosis. This iron-dependent lipid peroxidation cell death pathway aggravates airway epithelial injury in asthma (Yu *et al*., 2024). Recent studies in non-asthmatic models have shown that lactate can promote ACSL4 expression and direct lactylation of ACSL4, thereby enhancing its pro-ferroptotic activity (Xiang *et al*., 2025; Sun *et al*., 2025).

Although ACSL4 expression and ferroptosis have been repeatedly demonstrated in asthmatic airways, the post-translational regulation of ACSL4, particularly its lactylation, has never been explored in this context. Furthermore, whether the anti-asthmatic alkaloid

*Corresponding author: e-mail: ttzh_2360@163.com

ephedrine acts by modulating protein lactylation remains unclear. Therefore, this study aims to determine whether ephedrine suppresses ferroptosis by downregulating PKM2, thereby reducing lactate production and subsequent ACSL4 lactylation, which has not been previously reported in asthma model. In the present study, LPS-stimulated BEAS-2B cells and ovalbumin (OVA)-stimulated rats were employed as in vitro and in vivo asthma models to investigate whether PKM2 expression was modulated by EP., orchestrates ACSL4 lactylation and mitigates ferroptosis, thereby exerting salutary effects in asthma. Our findings will provide mechanistic evidence for EP's anti-asthmatic action and establish the PKM2-ACSL4 lactylation axis as a potential therapeutic target.

MATERIALS AND METHODS

Cell culture and grouping

BEAS-2B bronchial epithelial cells (SCSP-5067) were maintained in Dulbecco's modified Eagle's medium (DMEM)-10 % FBS and 1 % penicillin/streptomycin at 37 °C in a 5% CO_2 incubator. The medium was replaced every 2–3 days, and cells were passaged every 3–5 days when they reached approximately 80–90% confluence.

EP was aliquoted in dimethyl sulfoxide (DMSO) and kept at –20 °C. BEAS-2B cells received 48-h pre-treatment with 10 ng/mL lipopolysaccharide (LPS), graded concentrations of EP (1, 2.5, 5, 7.5, 10, 15 μg mL^{-1}), dexamethasone (DEX, 10 μM), or ferrostatin-1 (10 μM) (Liu *et al*., 2025; Wang *et al*., 2022; Li *et al*., 2021; Wang *et al*., 2023).

When cultures reached 90 % confluence, Lipofectamine 3000 (Invitrogen, USA) was used to transfect oe-PKM2 or empty vector, and si-ACSL4 or scrambled si-NC (GenePharma, Shanghai, China), according to the manufacturer's protocol; EP was added immediately after transfection, as per the experimental design.

CCK-8 assay for cell proliferation

Cell viability was measured using CCK-8 (Beyotime, C0037) following the manufacturer's protocol. 1×10^5 cells/well were seeded in 96-well plates, treated as indicated and absorbance at 450 nm was recorded.

TUNEL staining for apoptosis

Apoptosis was evaluated using a one-step TUNEL kit (Beyotime, C1086). After 4 % paraformaldehyde fixation, membranes were disrupted with 0.5 % Triton X-100 (20 min), followed by 1 h TUNEL labeling at 37 °C. Sections were then DAPI-counterstained for 10 min and imaged under a fluorescence microscope.

ELISA for TNF-α, IL-1β, IL-6

Specimens were immediately centrifuged (1 000 × g, 10 min, 4 °C), washed three times with ice-cold PBS and lysed by three freeze–thaw cycles (−80 °C → 37 °C) with intermittent sonication. After removing debris (1 000 × g, 10 min, 4 °C), TNF-α, IL-1β, and IL-6 in the clarified lysate were quantified using commercial ELISA kits (Bioswamp, Wuhan, China; HM10001, HM10206, HM10205) per the manufacturer's instructions.

ROS measurement

Cell pellets were harvested, and positive- and negative-control wells were prepared as specified for the ROS-Green fluorescence kit (Elabscience, Wuhan, E-BC-K138-F), and the reagent I working solution was prepared. After centrifugation, cells were resuspended in working solution and incubated 1 h at room temperature in the dark to allow probe loading. Subsequently, samples were centrifuged (1 000 × g, 10 min), washed three times with serum-free medium, resuspended and ROS levels determined.

Determination of Fe2+, MDA, SOD and LPO

Cell pellets were homogenized in ice-cold PBS, centrifuged at 12 000 × g for 10 min at 4 °C and the resulting supernatants were assayed for ferroptosis-associated analytes—ferrous ion (Fe^{2+}) by the fluorescent Fe^{2+} kit, malondialdehyde (MDA) by the colorimetric MDA kit, total superoxide dismutase (T-SOD) by the WST-1 colorimetric T-SOD kit and lipid hydroperoxides (LPO) by the fluorescent LPO kit—according to the respective protocols supplied with kits E-BC-F101, E-BC-K028-M, E-BC-K020-M and E-BC-F003 (Elabscience, Wuhan, China).

qPCR for PKM1 and PKM2 mRNA

TRIzol reagent (Absin, abs60154) was used for total-RNA isolation, followed by reverse transcription. Subsequent qPCR (40 cycles: 95 °C for 3 min; 95 °C for 30 s, 57 °C for 30 s, 72 °C for 30 s) was performed in strict accordance with the manufacturer's instructions. GAPDH served as the internal reference; PKM1 and PKM2 mRNA abundance was quantified via the 2-ΔΔCt method. Primer sequences(5′→3′):PKM1-F: GCCTCCAGTCACTCCACAGA,PKM1-R: CAGCACGGCATCCTTACACA;PKM2-F: ATTACCAGCGACCCCACAGAA,PKM2-R: ACGGCACCTTACACAGCACA;GAPDH-F: CGACCACTTTGTCAAGCTCA,GAPDH-R: AGGGGTCTACATGGCAACTG.

Western blot for PKM2 and ACSL4

Cells were lysed in RIPA buffer containing protease and phosphatase inhibitors and protein concentrations were determined by BCA assay. After SDS-PAGE and transfer, PVDF membranes were blocked with 10 % non-fat milk, incubated overnight at 4 °C with anti-PKM2 (1:500) or anti-ACSL4 (1:2,000; Thermo Fisher), followed by HRP-conjugated secondary antibody (1:10,000) for 2 h at room

temperature. Immunoreactive bands were visualized with ECL and quantified by ImageJ, with β-actin as loading control. For PKM2 cross-linking, tissue lysates were washed three times with PBS, treated with 500 μM DSS for 30 min at 37 °C and re-washed.

Lactate assay

Intracellular lactate was quantified with a microplate assay kit (Sangon Biotech, Shanghai, D799099). Cells (1×10^6) were mixed with extraction buffer I (10:1 v/v), sonicated on ice (300 W, 3 s on/7 s off, 3 min) and centrifuged at 12 000 × g for 10 min at 4 °C. Supernatant (0.8 mL) was mixed with 0.15 mL extraction buffer II, recentrifuged and the final supernatant was used for lactate determination.

Immunoprecipitation (IP) for ACSL4 lactylation

Cell lysates were prepared as directed by the IP kit manufacturer (P2193S, Beyotime, Shanghai, China). After lysis in an inhibitor-containing buffer, debris was removed by centrifugation (10 000 × g, 4 °C, 5 min). The supernatant was incubated with 4 μg of ACSL4 antibody (1:500) for 2 h at 4 °C with rotation, followed by 2 h incubation with IP buffer-prewashed Protein A/G agarose. Beads were washed three times, eluted in 2× Laemmli buffer (100 °C, 5 min) and analyzed by Western blot.

Experimental animals

Six- to eight-week-old male SPF Wistar rats (180–200 g) were supplied by the Hubei Provincial Center for Laboratory Animals [SCXK (Hubei) 2020-0018]. After arrival, animals were individually caged under a 12:12-h light–dark cycle with free access to chow and water. And a 7-day acclimation period preceded any experimental manipulation. The Institutional Animal Care and Use Committee approved procedures.

Rats were randomly assigned to either the control (Control) or model (OVA) group. Asthma was induced in the OVA group by intraperitoneal injection of 1 mg OVA (Sigma-Aldrich, Shanghai, China; lot 102433937) and 200 μg aluminum hydroxide ($Al(OH)_3$; Macklin, Shanghai, China; lot C12625445) in 0.5 mL PBS on days 0 and 7 (day 0 = first injection). From day 14 to day 42, the animals were exposed to aerosolized 1 % OVA for 30 min every other day in a closed chamber (Esmaeilpour *et al*., 2024). Successful modelling was defined by the appearance of tachypnoea, sneezing, ear- and face-scratching, restlessness, paroxysmal coughing and/or incontinence; the success rate was approximately 100 %. All rats fulfilling the criteria were used for subsequent experiments. Control animals inhaled PBS aerosol without OVA.

Rats that met the modelling criteria were re-assigned to the model (OVA), EP low-dose (OVA+EP-L), EP high-dose (OVA+EP-H) or dexamethasone (OVA+DEX) groups. OVA+EP-L and OVA+EP-H rats received EP at 15 mg/kg or 25 mg/kg, respectively, by oral gavage 1 h before each aerosol challenge (Wang *et al*., 2021a). Control and OVA rats received an equivalent volume of normal saline by gavage, whereas OVA+DEX rats received 0.5 mg/kg DEX intraperitoneally as a positive control (Ge *et al*., 2019). Body weight was recorded with an electronic balance (FA1004B; Shanghai Yueping Scientific Instrument Co., China) after the final treatment.

Assessment of asthma-related behavior in rats

After modeling and intervention, the mental state, stool/urine output, locomotor activity and water intake of each rat were observed and recorded. Asthma-related behavior was evaluated using an established scoring system comprising two components—asthma attack manifestations and asthma symptom severity; the sum of these two subscores was taken as the total asthma behavior score (Lizhong *et al*., 2024). The detailed criteria, adapted from a previously reported method (Lizhong *et al*., 2024), are presented in table 1.

Airway resistance (RL) and dynamic lung compliance (Cdyn)

Within 24 h of the final intervention, the FinePointe rodent pulmonary function system (Bucxo, USA) was prepared. Rats were then anesthetized by intraperitoneal injection of 2% pentobarbital sodium at 30 mg/kg body weight. A midline cervical tracheostomy was performed and the animal was positioned on the plethysmograph support plate. The tracheal cannula was connected to the pneumotachograph of the plethysmograph chamber. Intravenous access was established by inserting a scalp-vein needle into the common jugular vein. The chamber was then sealed to prevent air leaks. After a stable baseline was achieved, methacholine (Source Leaf Biotechnology, Shanghai, China; lot Z03A9H67294) was administered intravenously in doubling doses (0.025, 0.05, 0.1, 0.2 mg/kg) to provoke airway constriction. RL and Cdyn were continuously recorded (Nguyen *et al*., 2023; Cheng *et al*., 2024).

Specimen collection

After cervical dislocation, the thorax was opened. The lungs were lavaged in situ with sterile saline to obtain 1–1.5 mL bronchoalveolar lavage fluid (BALF), which was centrifuged and stored at –80 °C (Haier Biomedical, DW-86L419, Qingdao, China). The left lung was harvested, rinsed and fixed in 4 % paraformaldehyde; the right lung was snap-frozen at –80 °C.

Histopathology (hematoxylin–eosin)

Left lungs fixed in 4 % paraformaldehyde were dehydrated, paraffin-embedded (Leica EG 1150H; Leica Microsystems, Shanghai, China), sectioned at 4 μm, deparaffinized, rehydrated and stained with hematoxylin (3 min) and eosin (2 min) per the manufacturer's protocol (Baso HE kit, Zhuhai, China; lot C220201).

Table 1: Asthma-related behavioral scoring system

Score	Asthma attack manifestations	Asthma symptom severity
0 point	No nose scratching or rubbing	No obvious symptoms
1 point	Nose scratching or rubbing 1–3 times	Mild symptoms: Occasional tachypnea, slight irritability
2 points	Nose scratching or rubbing 4–6 times	Moderate symptoms: Persistent tachypnea, markedly increased respiratory rate
3 points	Nose scratching or rubbing ≥7 times	Severe symptoms: Dyspnea with nodding respiration, cyanosis

The total asthma behavior score was calculated as the sum of the scores for attack manifestations and symptom severity, ranging from 0 to 6.

Sections were mounted and examined under light microscopy for histopathological changes.

ELISA for TNF-α, IL-1β and IL-6 in BALF

Levels of TNF-α, IL-1β and IL-6 in centrifuged BALF were quantified with commercial rat ELISA kits (Bioswamp, Wuhan, China; cat. nos. RA20607, RA20020 and RA20035) according to the manufacturer's instructions.

Lung tissue Fe^{2+}, MDA, SOD and LPO

Lung tissue (0.1 g) was homogenized in 0.9 mL Reagent-5, centrifuged (12 000 × g, 10 min, 4 °C) and the supernatant assayed for Fe^{2+}, MDA, T-SOD and LPO using colorimetric kits (E-BC-K773-M, E-BC-K025-M, E-BC-K020-M and E-BC-K176-M, respectively; Elabscience, Wuhan, China) per protocol.

Lactate measurement

Tissue was mixed with extraction buffer-I at 1:10 (w/v), homogenized on ice and centrifuged at 12 000 × g, 4 °C, 10 min. An 0.8 mL aliquot of supernatant was combined with 0.15 mL extraction buffer-II, recentrifuged under identical conditions and the final supernatant used for lactate determination.

Immunohistochemistry for lactylation, PKM2 and ACSL4

Lung tissue fixed in 4 % formalin was paraffin-sectioned (4 μm), subjected to antigen retrieval and blocked with 5 % goat serum (1 h). Sections were incubated overnight at 4 °C with anti-PKM2 (1:100), pan-lysine lactylation (1:50) or anti-ACSL4 (1:100), followed by HRP-secondary (1:4000, 2 h) and DAB visualization. Slides were counterstained with hematoxylin and positive signals quantified (Image-Pro Plus 6.0).

Statistical analysis

All statistical analyses were conducted using SPSS software. Comparisons between two independent groups were performed using an unpaired Student's t-test. For comparisons involving more than two groups, one-way ANOVA was applied, followed by Bonferroni correction to correct for multiple comparisons. $P < 0.05$ indicated statistical significance.

RESULTS

EP alleviates LPS-induced BEAS-2B cell injury

CCK-8 assays showed that LPS exposure markedly reduced cell proliferation versus the Ctrl group. Co-treatment with DEX or EP at 1–15 μg/mL attenuated this reduction, with the 10 μg/mL EP dose achieving the most pronounced recovery, approximating the DEX level ($P < 0.05$) (Fig. 1A). This concentration was therefore adopted for further studies. Flow cytometric apoptosis and ELISA analyses showed that LPS markedly increased the apoptotic rate and elevated TNF-α, IL-1β, and IL-6 levels relative to Ctrl. Both EP (10 μg/mL) and DEX reversed these elevations, lowering apoptosis and cytokine concentrations ($P < 0.05$) (Figs. 1B, C).

EP suppresses LPS-induced ferroptosis in BEAS-2B cells

Relative to the Ctrl group, LPS challenge provoked a significant surge in intracellular ROS, Fe^{2+}, MDA and LPO concomitant with a pronounced decline in SOD activity ($P < 0.05$) (Fig. 2A). Relative to the LPS group, both LPS+EP and LPS+Fer-1 treatments markedly decreased ROS, Fe^{2+}, MDA and LPO contents and restored SOD activity ($P < 0.05$) (Fig. 2B). These data indicate that EP, akin to Fer-1, inhibits LPS-triggered ferroptosis in BEAS-2B cells.

PKM2 overexpression reverses the protective effect of EP against LPS-challenged BEAS-2B cells

The experimental design is depicted in figure 3A. qPCR and Western blot analyses showed that LPS up-regulated PKM2 expression, whereas EP treatment suppressed PKM2 levels ($P < 0.05$) (Fig. 3B). PKM2 was more abundant than PKM1 in BEAS-2B cells. Compared with LPS alone, LPS+EP significantly increased cell viability, reduced the apoptotic rate, and lowered TNF-α, IL-1β, and IL-6 release; concomitantly, ROS, Fe^{2+}, MDA, and LPO contents were decreased, and SOD activity was restored ($P < 0.05$). PKM2 overexpression reversed these beneficial effects: relative to LPS+EP+vector, the LPS+EP+PKM2 group exhibited reduced cell viability, elevated apoptosis, higher TNF-α, IL-1β and IL-6 concentrations, increased ROS, Fe^{2+}, MDA and LPO levels and diminished SOD activity ($P < 0.05$) (Figs. 4C–G).

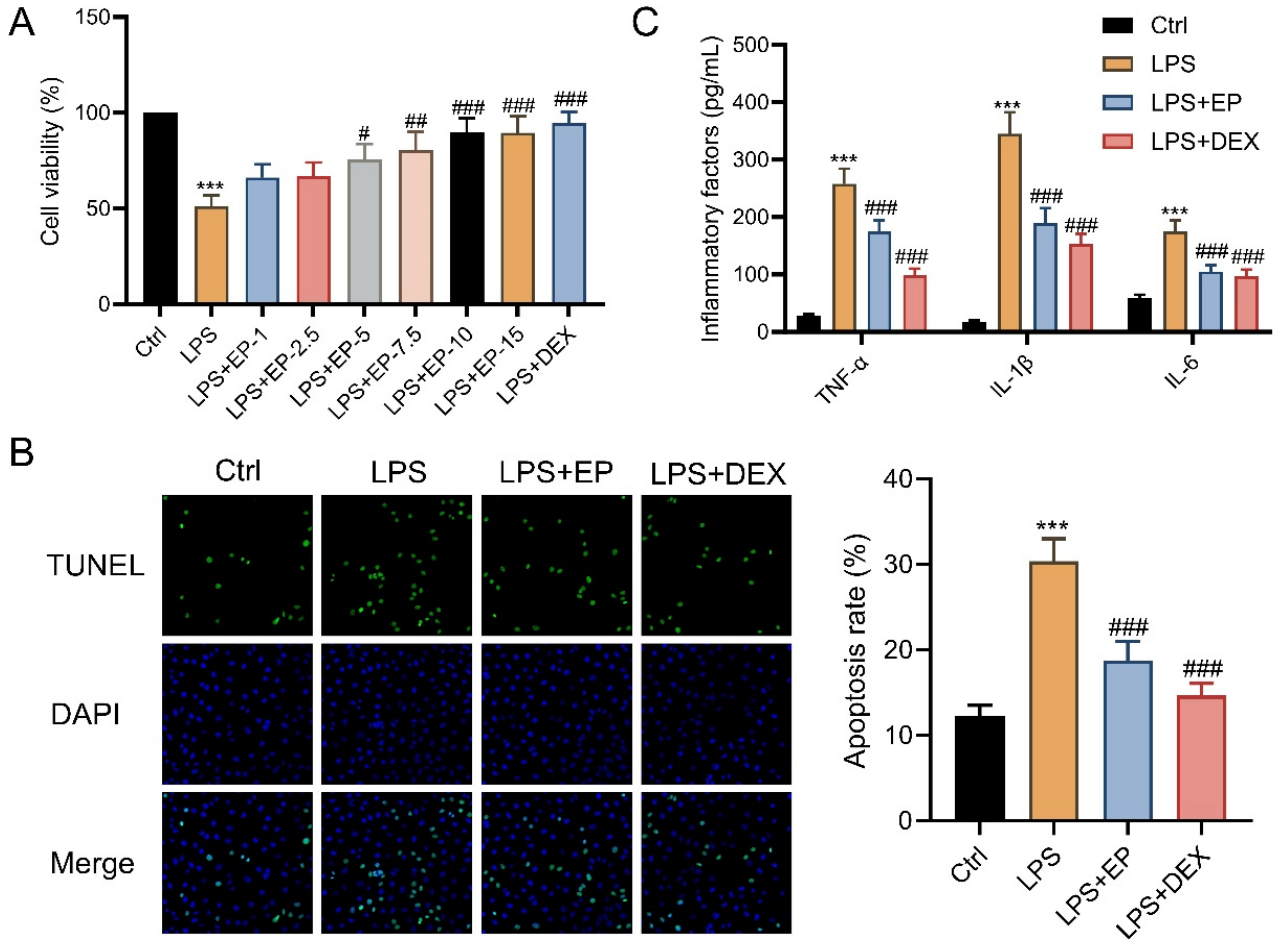

Fig. 1: Ephedrine (EP) attenuates LPS-induced BEAS-2B cell injury.
(A) Cell viability determined by CCK-8 assay. Data are mean ± SD (n = 6 independent experiments); (B) Apoptotic rate quantified by TUNEL staining (representative images and quantification). Data are mean ± SD (n = 6); (C) Levels of TNF-α, IL-1β and IL-6 in culture supernatants measured by ELISA. Data are mean ± SD (n = 6).
*P < 0.001 vs. Ctrl group; #P < 0.05, ##P < 0.01, ###P < 0.001 vs. LPS group (Bonferroni correction).

PKM2 overexpression enhances lactylation and expression of ACSL4

In LPS-stimulated BEAS-2B cells, PKM2 overexpression significantly increased intracellular lactate levels, total ACSL4 protein abundance and ACSL4 lactylation relative to the LPS+vector group (P < 0.05) (Figs. 4A–C).

Inhibition of ACSL4 lactylation reverses PKM2-driven injury in LPS-challenged BEAS-2B cells

In the LPS-induced BEAS-2B injury model, combined modulation of PKM2 and ACSL4 expression was performed to evaluate effects on cell damage and ferroptosis. Compared with the LPS+vector group, LPS+oe-PKM2 exhibited elevated ACSL4 protein and ACSL4 lactylation, reduced cell viability, increased apoptotic rate and TNF-α, IL-1β, IL-6 release, augmented ROS, Fe^{2+}, MDA and LPO levels and decreased SOD activity. Relative to LPS+oe-ACSL4+vector, simultaneous ACSL4 silencing reversed the detrimental effects of PKM2 overexpression: ACSL4 abundance and lactylation declined, cell viability recovered, apoptosis and cytokine concentrations decreased, ROS, Fe^{2+}, MDA and LPO contents were lowered and SOD activity was restored (P < 0.05) (Figs. 5A–F).

EP mitigates OVA-triggered asthmatic manifestations in rats

The animal protocol is outlined in figure 6A. General observation revealed that control rats displayed normal mental status, agile movement, glossy fur, and regular food and water intake, along with normal urination and defecation. Rats in the OVA group exhibited frequent wheezing, nose-rubbing, irritability, bilateral alopecia around the nostrils with scratch marks, obvious abdominal breathing, listlessness and delayed response. After aerosol challenge, these manifestations were markedly attenuated in the OVA+EP-L, OVA+EP-H and OVA+DEX groups compared with the OVA group.

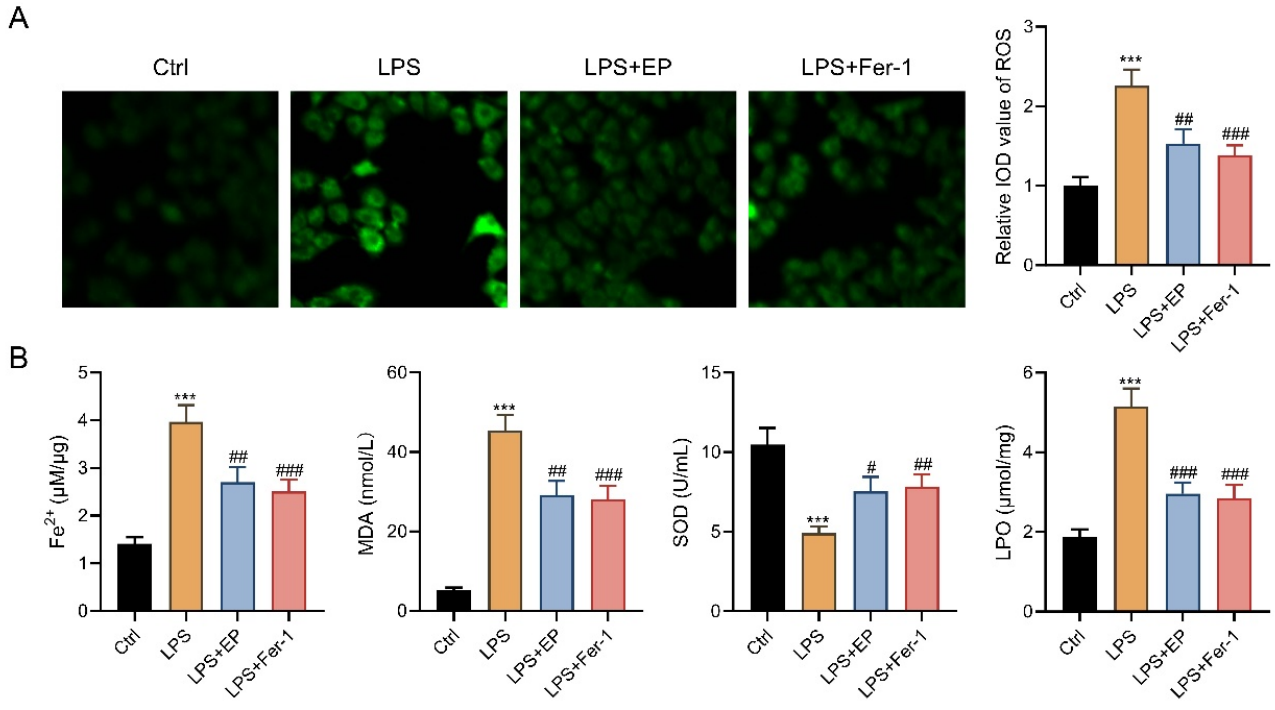

Fig. 2: EP suppresses LPS-induced ferroptosis in BEAS-2B cells.
(A) Intracellular ROS levels measured by fluorescence assay; (B) Levels of Fe^{2+}, MDA, SOD activity and LPO. All data are mean ± SD (n = 6). ***P < 0.001 vs. Ctrl; #P < 0.05, ##P < 0.01, ###P < 0.001 vs. LPS (Bonferroni correction).

Body weight and behavioral score measurements showed that OVA rats had lower body weight and significantly higher behavioral scores versus controls (P < 0.05); EP or DEX administration reversed these changes, increasing body weight and reducing behavioral scores (P < 0.05) (Figs. 6B, C). Lung-function tests demonstrated that, relative to controls, OVA rats exhibited elevated RL and reduced Cdyn at every methacholine concentration (P < 0.05); EP or DEX treatment decreased RL and increased Cdyn at each dose (P < 0.05) (Figs. 6D, E). HE staining of lung sections showed intact pulmonary architecture without inflammatory infiltration in controls. OVA rats displayed disrupted architecture, narrowed airways, massive interstitial inflammatory-cell infiltration and partial alveolar collapse. These alterations were less severe in the OVA+EP-L, OVA+EP-H and OVA+DEX groups, with reduced inflammatory infiltration and no evident alveolar collapse (Fig. 6F). ELISA of bronchoalveolar lavage fluid revealed up-regulated TNF-α, IL-1β and IL-6 levels in OVA rats compared with controls (P < 0.05); these cytokines were down-regulated after EP or DEX treatment (P < 0.05) (Fig. 6G). Collectively, EP and DEX produced comparable improvements in OVA-induced asthmatic manifestations.

EP suppresses ferroptosis and down-regulates PKM2 and ACSL4 in lung tissue of OVA-challenged rats

Compared with the Control group, OVA exposure significantly elevated pulmonary ROS, Fe^{2+}, MDA and LPO levels while reducing SOD activity (P < 0.05). These changes were reversed by EP-L, EP-H, or DEX, which decreased ROS, Fe^{2+}, MDA and LPO contents and restored SOD activity (P < 0.05) (Figs. 7A–B), indicating that EP and DEX inhibit OVA-induced ferroptosis in lung tissue.

Measurement of pulmonary lactate, PKM2, and ACSL4 revealed higher lactate levels and increased PKM2 and ACSL4 expression in the OVA group compared with controls. Relative to the OVA group, EP-L, EP-H and DEX treatments lowered pulmonary lactate concentration and reduced PKM2 and ACSL4 abundance (P < 0.05) (Figs. 7C–D).

DISCUSSION

Asthma is regarded as a heterogeneous, multifactorial respiratory disease driven by multiple inflammatory cytokines; viral infection, allergen or irritant exposure, psychological stress and genetic predisposition all contribute to its onset (Ramsahai *et al*., 2019, Gans and Gavrilova, 2020). Current therapy aims to relieve airway obstruction and reduce inflammation, relying mainly on bronchodilators for acute relief and maintenance drugs to preserve quality of life. Disease control is achievable, but cure remains elusive (Kwah and Peters, 2019). Identification of novel agents and therapeutic targets is therefore essential.

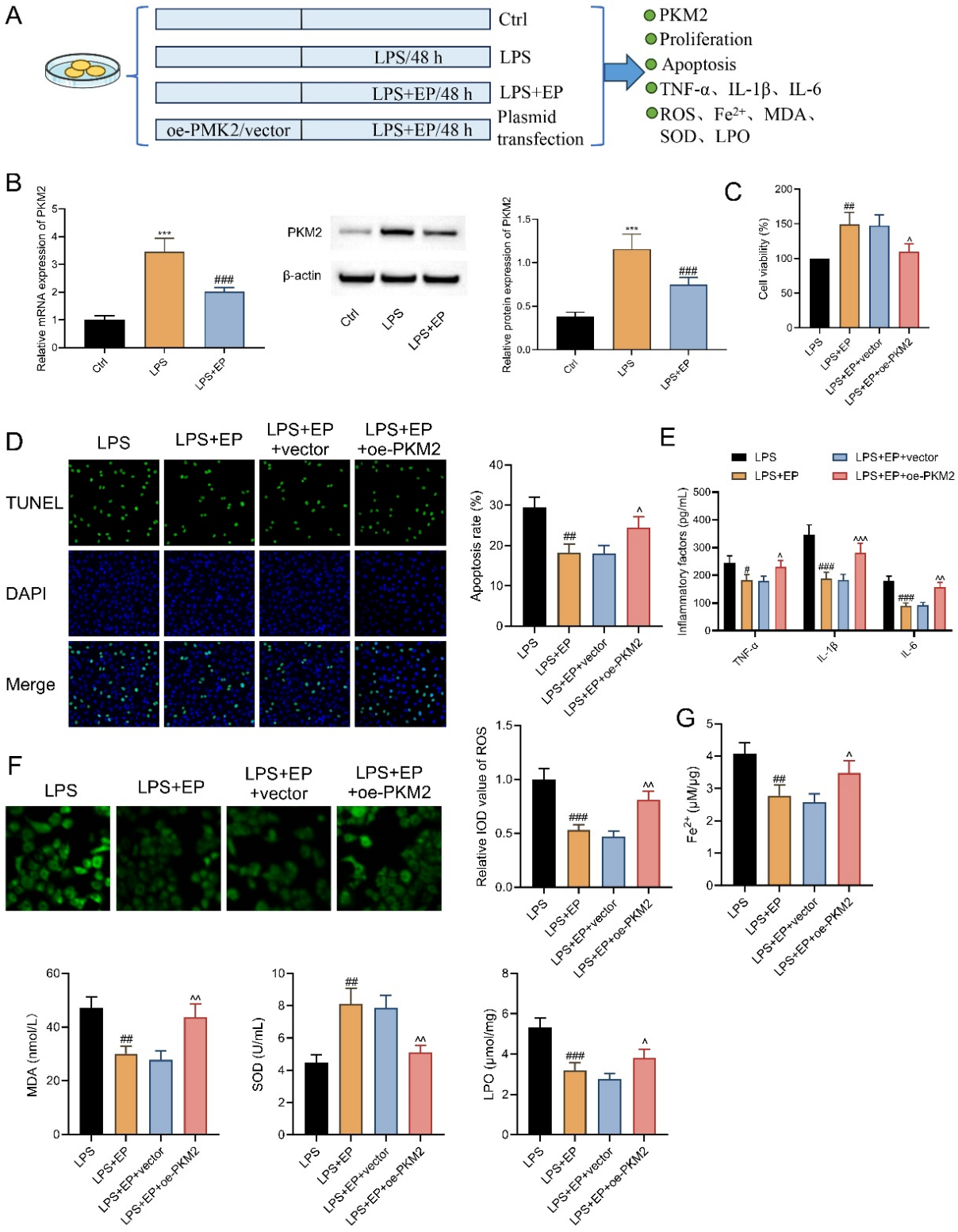

Fig. 3: PKM2 overexpression reverses the protective effect of EP in LPS-challenged BEAS-2B cells.
(A) Experimental scheme; (B) Relative PKM2 mRNA and protein levels. Data are mean ± SD (n = 3); (C) Cell viability (CCK-8). Data are mean ± SD (n = 6); (D) Apoptosis (TUNEL). Data are mean ± SD (n = 6); (E) TNF-α, IL-1β, IL-6 (ELISA). Data are mean ± SD (n = 6); (F) ROS levels. Data are mean ± SD (n = 6); (G) Fe^{2+}, MDA, SOD, LPO. Data are mean ± SD (n = 6). *P < 0.001 vs. Ctrl; ###P < 0.001 vs. LPS; ^P < 0.05, ^^P < 0.01, ^^^P < 0.001 vs. LPS+EP+vector (Bonferroni correction).

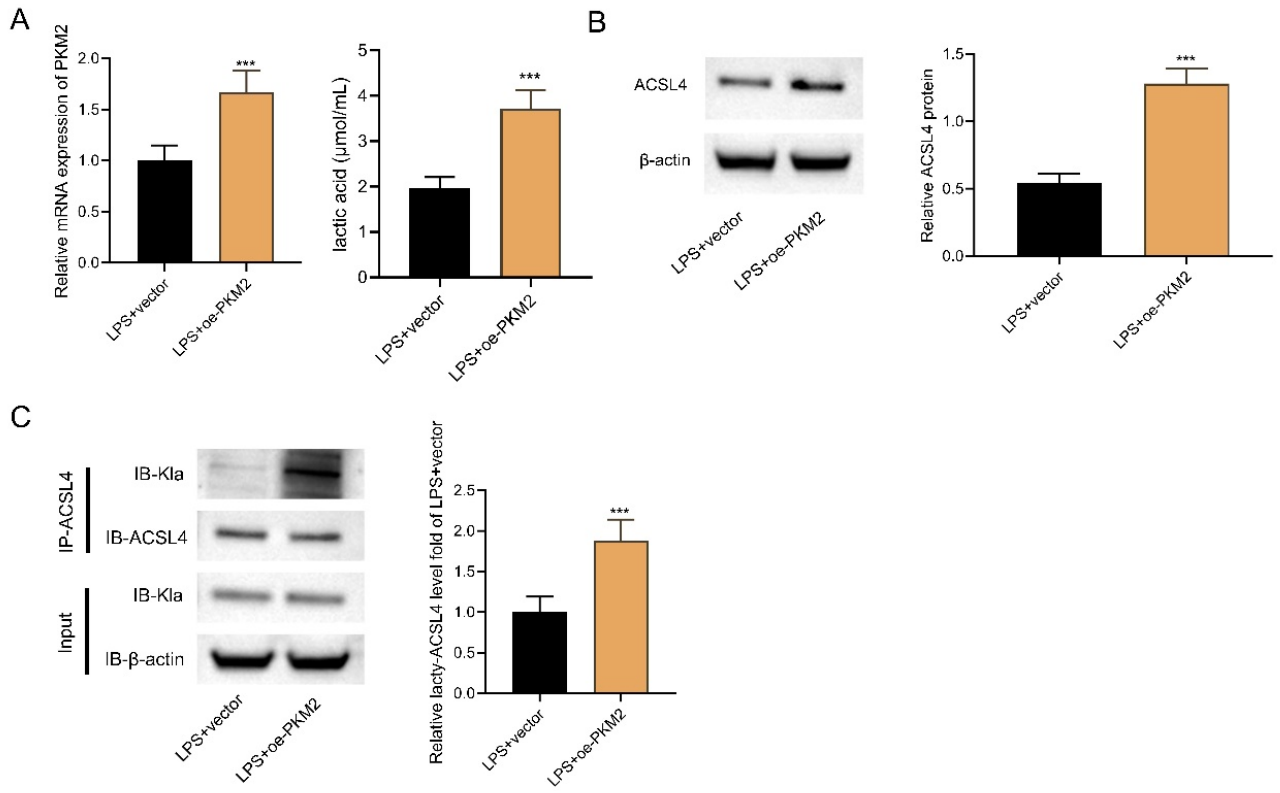

Fig. 4: PKM2 overexpression promotes ACSL4 lactylation and expression.
(A) Intracellular lactate levels measured by colorimetric kit. Data are mean ± SD (n = 6); (B) ACSL4 protein expression by Western blot. Data are mean ± SD (n = 3); (C) ACSL4 lactylation assessed by co-immunoprecipitation (IP) followed by Western blot. Data are mean ± SD (n = 3). *P < 0.05, **P < 0.01 vs. LPS+vector (Bonferroni correction).

In recent years, bioactive compounds derived from traditional Chinese herbs have been recognized as a promising therapeutic strategy for asthma (Yuan *et al*., 2022, Wang *et al*., 2021b). Ephedra sinica, clinically used for respiratory tract infections and bronchial asthma (Zheng *et al*., 2023), yields the alkaloid EP whose beneficial effects in asthma have been documented. EP combined with heparin II attenuates airway remodeling and inflammation in asthmatic rats (Wang *et al*., 2021a) and recent work showed that EP limits lung injury by targeting PKM2, thereby suppressing macrophage glycolysis and M1 polarization (Xiang *et al*., 2024). In the current study, an *in-vitro* asthma model was established by LPS stimulation of BEAS-2B cells and an *in-vivo* rat model was generated by OVA sensitization and challenge. EP intervention was compared with DEX as positive control. EP significantly mitigated LPS-induced cellular injury and inflammatory responses and concurrently ameliorated OVA-driven asthmatic manifestations in rats. These findings position EP as a therapeutic potential for the treatment of asthma. In contrast to most previous studies that focused on the occurrence of ferroptosis or ACSL4 expression in asthma, This study provides three distinct advances. Firstly, it identifies lactylation as a previously unrecognized activator of ACSL4 in asthmatic epithelial cells. Secondly, it establishes PKM2 as a direct upstream regulator of ACSL4 lactylation via lactate. Thirdly, it reveals that ephedrine acts as a pharmacological breaker of this PKM2-to-lactate-to-lactylation-to-ferroptosis cascade.

Ferroptosis is an iron-driven, regulated form of cell demise characterized by iron accumulation, ROS generation and subsequent lipid peroxidation that compromises membrane integrity (Jiang *et al*., 2021). It is closely linked to asthma and amplifies airway inflammation (Liu *et al*., 2023; Li *et al*., 2023b). Natural products targeting ferroptosis show promise in respiratory diseases (Xu *et al*., 2024; Chen *et al*., 2024b; Sun *et al*., 2024), yet the effect of EP on ferroptosis had not been explored. In both LPS-challenged BEAS-2B cells and OVA-challenged rats, EP markedly inhibited ferroptosis by reducing oxidative stress and lipid peroxidation, preserving membrane integrity and limiting pulmonary oxidative damage. These findings provide mechanistic support for the anti-asthmatic action of EP through modulation of ferroptosis.

Multiple studies have verified the pivotal role of PKM2 in cancer therapy (Zhu *et al*., 2021; Li *et al*., 2023a). Beyond oncogenesis, PKM2 also drives inflammatory progression in diverse diseases.

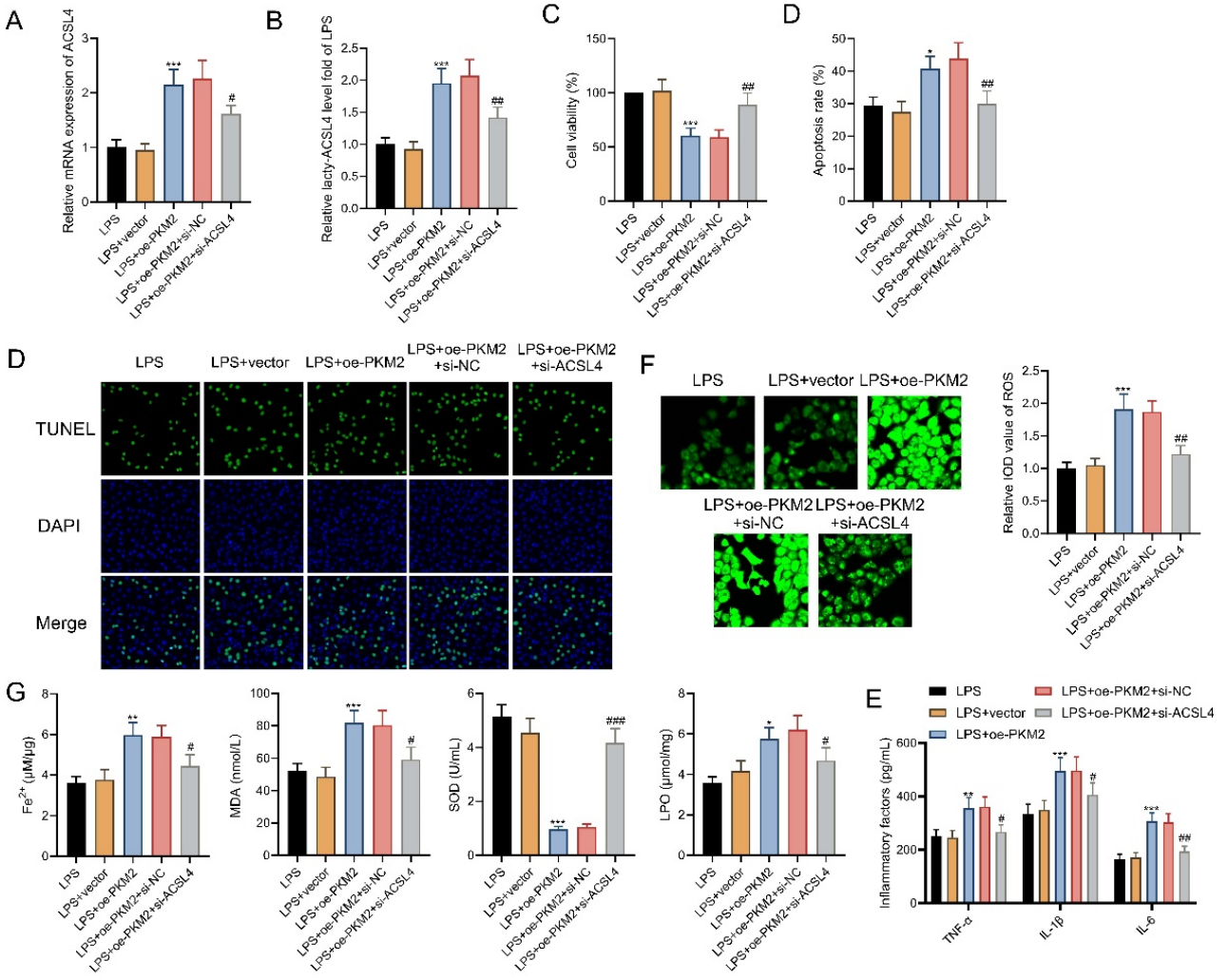

Fig. 5: Inhibition of ACSL4 lactylation reverses PKM2 overexpression-induced injury in LPS-challenged BEAS-2B cells.

(A) ACSL4 protein expression (Western blot). Data are mean ± SD (n = 3); (B) ACSL4 lactylation (IP). Data are mean ± SD (n = 3); (C) Cell viability (CCK-8). Data are mean ± SD (n = 6); (D) Apoptosis (TUNEL). Data are mean ± SD (n = 6); (E) Cytokines (TNF-α, IL-1β, IL-6). Data are mean ± SD (n = 6); (F) ROS levels. Data are mean ± SD (n = 6); (G) Fe^{2+}, MDA, SOD, LPO. Data are mean ± SD (n = 6). *P < 0.05, **P < 0.01, ***P < 0.001 vs. LPS+vector; #P < 0.05, ##P < 0.01, ###P < 0.001 vs. LPS+oe-PKM2+vector (Bonferroni correction).

For instance, quercetin attenuated LPS-induced lung injury by curbing PKM2 nuclear translocation and consequently suppressing NLRP3 inflammasome activation (Chen *et al*., 2022). PKM2 knock-down dampened glycolysis and reduced macrophage-mediated inflammation, offering a novel strategy against acute kidney failure (Fan *et al*., 2021). PKM2 up-regulation cooperated with mitophagy to enhance cigarette-smoke-extract-triggered inflammatory responses and epithelial–mesenchymal transition in bronchial epithelial cells (Li *et al*., 2022). In the present study, an LPS-challenged BEAS-2B cell line served as an in-vitro asthma model. Functional assays targeting PKM2 revealed that its over-expression markedly potentiated ferroptosis and consequent airway epithelial injury, whereas EP reversed these effects by down-regulating PKM2, thereby attenuating ferroptosis and cellular damage.

Lactylation can alter protein conformation, modulate gene transcription and regulate expression of related genes (Jiang *et al*., 2024). In OVA-allergic rats, heightened glycolysis increases lactate levels, promotes protein lactylation, and synergizes with pyroptosis to aggravate inflammation and airway damage (Chen *et al*., 2024a); thus, blocking lactate generation or lactylation may offer a new therapeutic avenue. PKM2-driven lactate has been shown to facilitate H3K18 lactylation, induce Tgfb1 transcription and exacerbate renal fibrosis via Smad3 (Xiang *et al*., 2025).

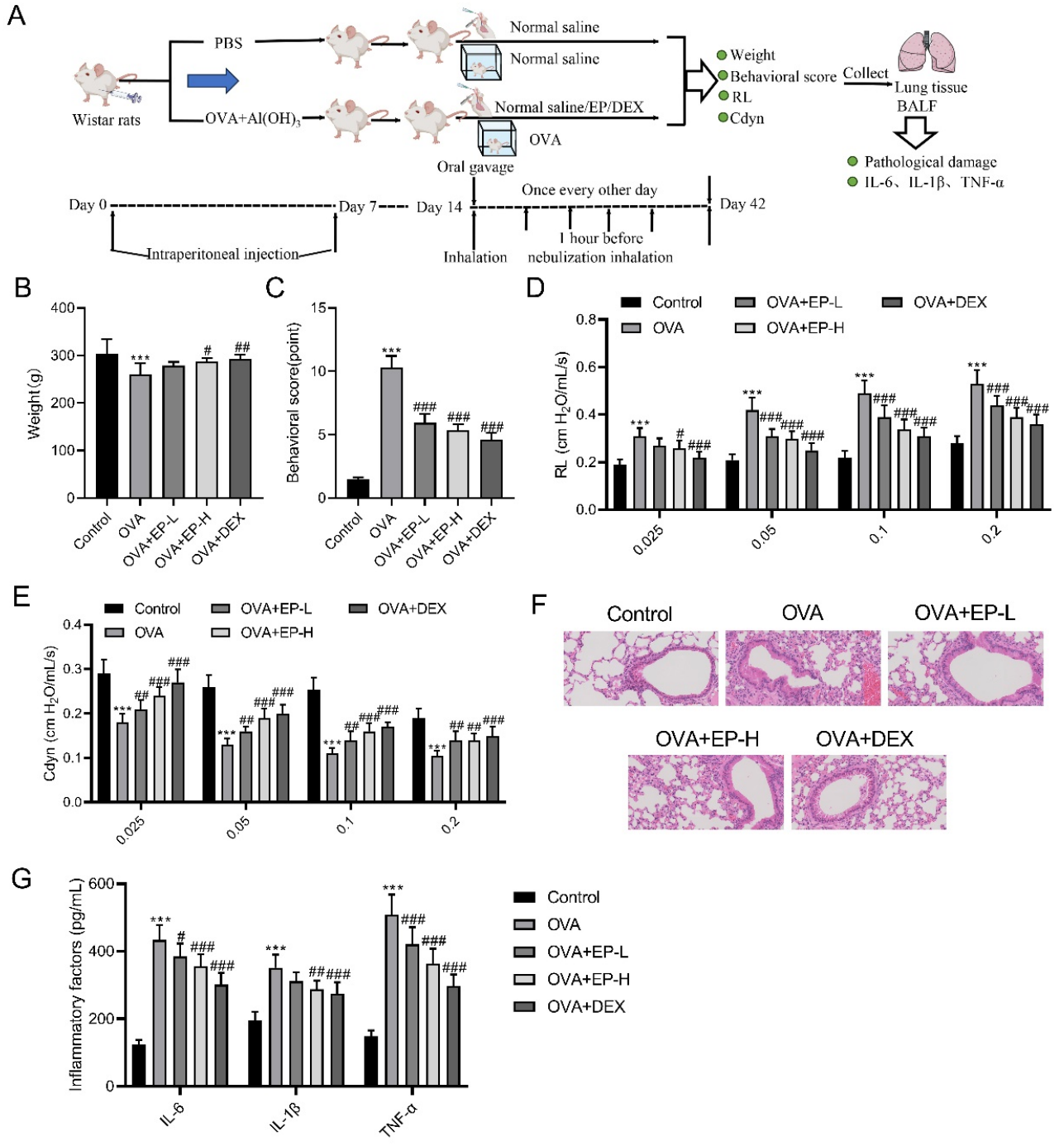

Fig. 6: EP ameliorates OVA-induced asthmatic manifestations in rats.
(A) Experimental protocol; (B) Body weight. Data are mean ± SD (n = 6 per group); (C) Asthma behavioral score. Data are mean ± SD (n = 6); (D) Airway resistance (RL) at increasing methacholine doses. Data are mean ± SD (n = 6); (E) Dynamic compliance (Cdyn). Data are mean ± SD (n = 6); (F) Representative hematoxylin-eosin (HE) staining of lung sections (scale bars = 100 μm); (G) BALF levels of TNF-α, IL-1β, IL-6 measured by ELISA. Data are mean ± SD (n = 6). *P < 0.001 vs. Control; #P < 0.05, ##P < 0.01, ###P < 0.001 vs. OVA (Bonferroni correction).

In heavy-metal-induced pulmonary toxicity, lactate accumulation enhances H3K18 lactylation, elevates ROS and amplifies epithelial oxidative injury (Xie *et al*., 2025). During disc degeneration, H3K18 lactylation promotes ACSL4 transcription and ACSL4 lactylation, augmenting lipid peroxidation and ferroptosis (Sun *et al*., 2025); enhanced ACSL4 activity further propagates airway inflammation and asthmatic pathology (Tang *et al*., 2023).

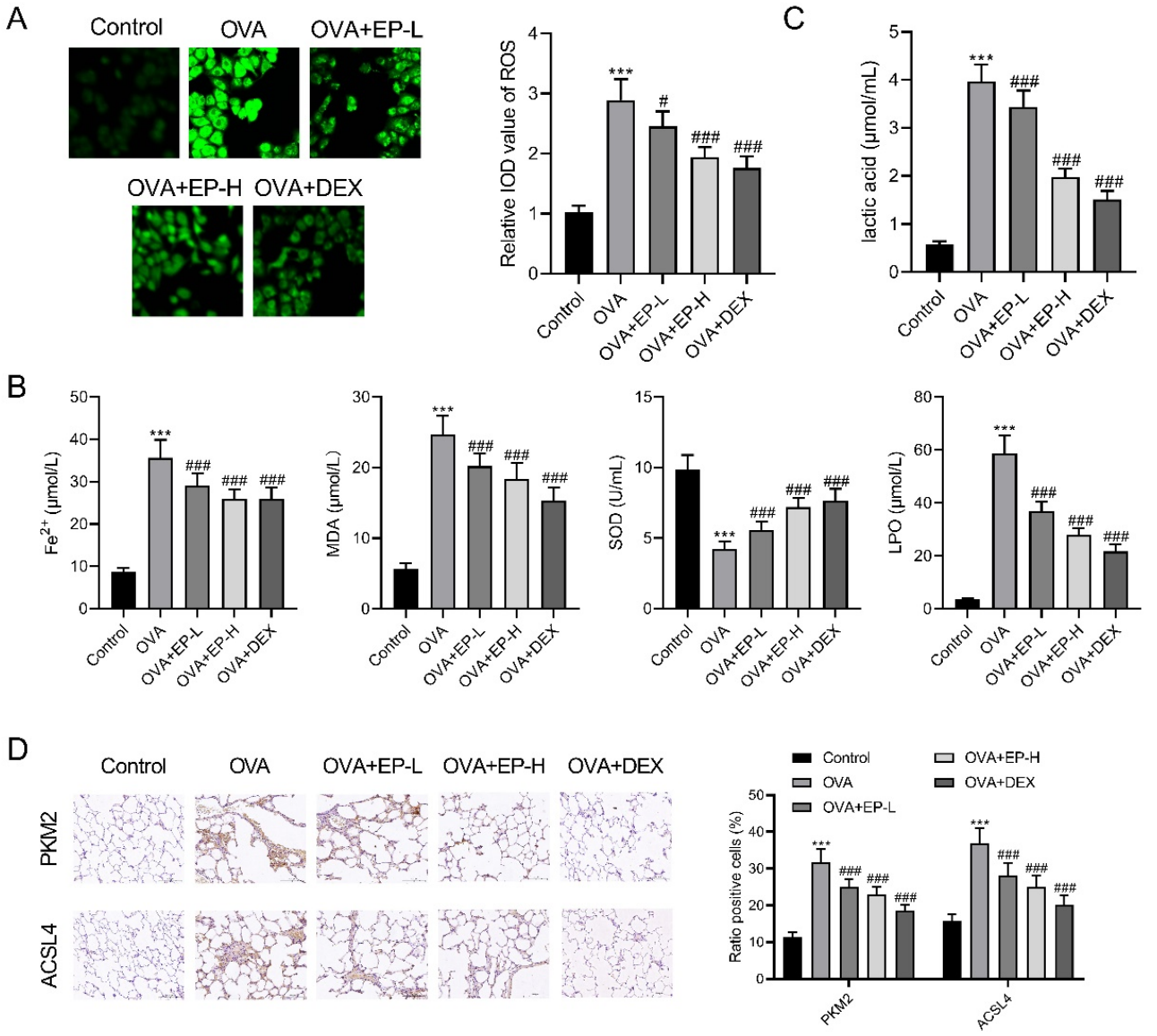

Fig. 7: EP suppresses ferroptosis and reduces lactate, PKM2 and ACSL4 in lung tissue of OVA-challenged rats. (A) Pulmonary ROS levels. Data are mean ± SD (n = 6); (B) Pulmonary Fe^{2+}, MDA, SOD, LPO. Data are mean ± SD (n = 6); (C) Pulmonary lactate levels. Data are mean ± SD (n = 6); (D) Representative immunohistochemistry (IHC) staining of PKM2 and ACSL4 in lung sections (scale bars = 50 μm). Quantification (mean optical density) is shown below. Data are mean ± SD (n = 6). *P < 0.001 vs. Control; #P < 0.05, ###P < 0.001 vs. OVA (Bonferroni correction).

We found that PKM2 elevation increased lactate production, up-regulated ACSL4 expression and lactylation and intensified ferroptosis and epithelial injury. EP, by suppressing PKM2 and lactate generation, reduced ACSL4 lactylation, attenuated ferroptosis and airway inflammation and improved asthmatic manifestations.

Several limitations should be noted. First, the OVA-induced asthma model does not fully mimic the heterogeneity of human asthma. Similarly, BEAS-2B cells are immortalized and may not fully represent primary airway epithelial cells. Second, we did not map the specific lysine residues on ACSL4 that undergo lactylation, a task requiring future mass spectrometry analysis. Third, the long-term safety and optimal dosing of ephedrine for targeting this pathway require further investigation beyond its established bronchodilator use. Future studies addressing these limitations will strengthen the clinical relevance of our findings.

CONCLUSION

In summary, we delineate a PKM2–ACSL4 lactylation axis that modulates ferroptosis and asthmatic progression and we identify EP as a pharmacologic inhibitor of this pathway (mechanistic schema in figure 8).

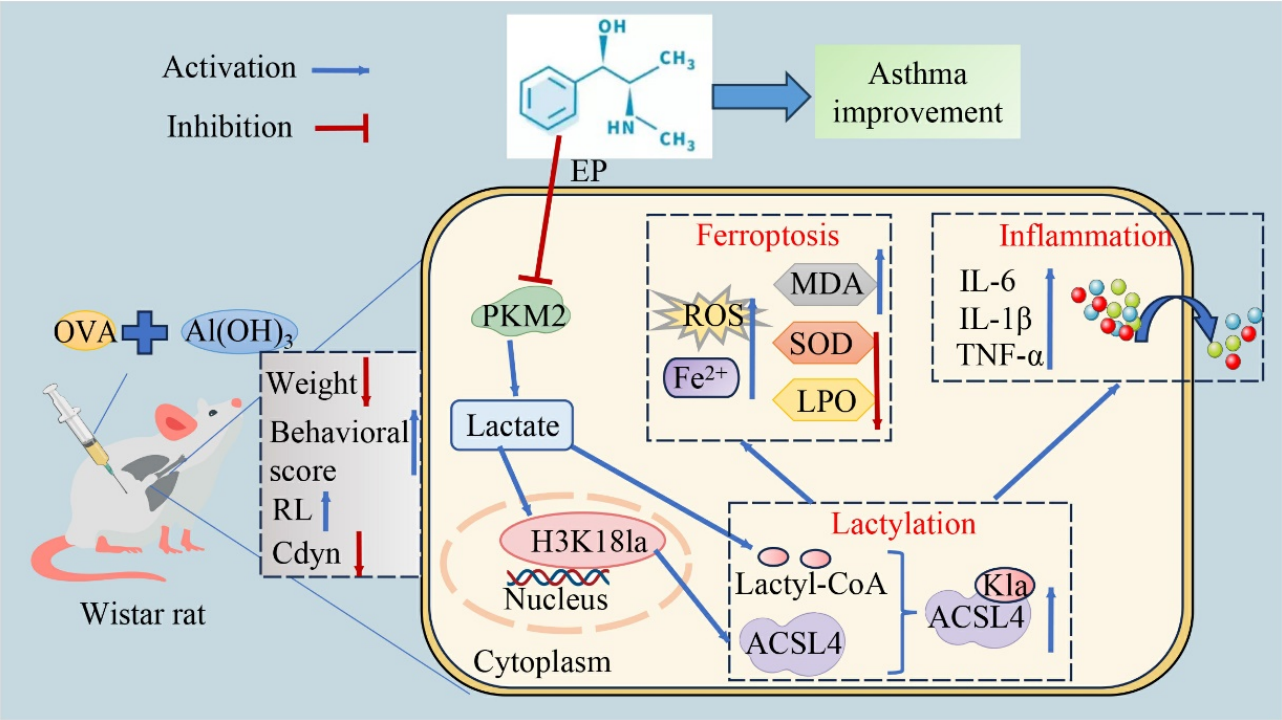

Fig. 8: Mechanism diagram of this study.

While the OVA rat model recapitulates key features of human asthma, it cannot fully mirror the complexity of the human disease. Future pre-clinical and clinical investigations are essential to confirm the therapeutic potential and safety profile of EP, facilitating its clinical translation for asthma management.

Acknowledgements
The authors are grateful for the support received during this study. We would like to thank the Lanzhou University Second Hospital, for providing the necessary facilities and research environment.

Author's contributions
Conceptualization, Lanting Zhao; methodology, Lanting Zhao and Rong Xia; formal analysis, Shuang Zeng; investigation, XiaoXia Yan; data curation, Lanting Zhao; writing—original draft preparation, Lanting Zhao; writing—review and editing, Lanting Zhao and Rong Xia; project administration, Lanting Zhao. All authors have read and agreed to the published version of the manuscript.

Funding
There was no funding

Data availability statement
The datasets generated during and/or analyzed during the current study are available from the corresponding author on reasonable request.

Ethical approval
This study was conducted in accordance with international, national, and institutional guidelines for humane animal treatment and relevant legislation. Specifically, all procedures involving mice were approved by the Animal Ethical Care Committee of The Lanzhou University Second Hospital (AECC-2023-015). This study was performed in adherence with the ARRIVE guidelines. See supplementary file for the ARRIVE checklist.

Conflict of interest
The authors declare no conflict of interest.

Supplementary data
https://www.pjps.pk/uploads/2026/07/SUP1784797191.pdf

REFERENCES

Chen LL, Song C, Zhang Y, Li Y, Zhao YH, Lin FY, Han DD, Dai MH, Li W and Pan PH (2022). Quercetin protects against LPS-induced lung injury in mice via SIRT1-mediated suppression of PKM2 nuclear accumulation. *Eur. J. Pharmacol.*, **936**: 175352.

Chen N, Xie QM, Song SM, Guo SN, Fang Y, Fei GH and Wu HM (2024). Dexamethasone protects against asthma via regulating Hif-1α-glycolysis-lactate axis and protein lactylation. *Int. Immunopharmacol.*, **131**: 111791.

Chen T, Ding L, Zhao M, Song S, Hou J, Li X, Li M, Yin K, Li X and Wang Z (2024). Recent advances in the

potential effects of natural products from traditional Chinese medicine against respiratory diseases targeting ferroptosis. *Chin. Med.*, **19**(1): 49.

Cheng L, Xiang S, Yu Q, Yu T, Sun P, Ye C and Xue H (2024). Paeoniflorin inhibits PRAS40 interaction with Raptor to activate mTORC1 to reverse excessive autophagy in airway epithelial cells for asthma. *Phytomedicine*, **134**: 155946.

Esmaeilpour K, Jafari E, Rostamabai F, Khaleghi M, Akhgarandouz F, Hosseini M, Najafipour H, Khodadoust M, Sheibani V and Rajizadeh MA (2024). Myrtenol inhalation mitigates asthma-induced cognitive impairments: An electrophysiological, behavioral, histological and molecular study. *Mol. Neurobiol.*, **61**(7): 4891-4907.

Fan XG, Pei SY, Zhou D, Zhou PC, Huang Y, Hu XW, Li T, Wang Y, Huang ZB, Li N (2021). Melittin ameliorates inflammation in mouse acute liver failure via inhibition of PKM2-mediated Warburg effect. *Acta Pharmacol Sin.*, **42**(8): 1256-1266.

Gad MZ, Azab SS, Khattab AR and Farag MA (2021). Over a century since ephedrine discovery: An updated revisit to its pharmacological aspects, functionality and toxicity in comparison to its herbal extracts. *Food Funct.*, **12**(20): 9563-9582.

Gans MD and Gavrilova T (2020). Understanding the immunology of asthma: Pathophysiology, biomarkers and treatments for asthma endotypes. *Paediatr. Respir. Rev.*, **36**: 118-127.

Ge Y, Cheng R, Sun S, Zhang S, Li L, Jiang J, Yang C, Xuan X and Chen J (2019). Fangxiao Formula alleviates airway inflammation and remodeling in rats with asthma via suppression of transforming growth factor-β/Smad3 signaling pathway. *Biomed. Pharmacother.*, **119**: 109429.

Hu Y, Wang M, Xie J, Jiao L, Ding Y and Luo Y (2024). Exposure to ephedrine attenuates Th1/Th2 imbalance underlying OVA-induced asthma through airway epithelial cell-derived exosomal lnc-TRPM2-AS. *Chin. J. Nat. Med.*, **22**(6): 530-540.

Huang L, Zhao B, Li Q, Wu J, Jiang H and Li Q (2021). Ephedrine alleviates middle cerebral artery occlusion-induced neurological deficits and hippocampal neuronal damage in rats by activating PI3K/AKT signaling pathway. *Bioengineered*, **12**(1): 4136-4149.

Jiang X, Stockwell BR and Conrad M (2021). Ferroptosis: Mechanisms, biology and role in disease. *Nat. Rev. Mol. Cell Biol.*, **22**(4): 266-282.

Jiang X, Yang Y, Li X, Li T, Yu T and Fu X (2024). Lactylation: An innovative approach to disease control. *Aging Dis.*, **16**(4): 2130-2150.

Jing F, Zhang J, Zhang H and Li T (2025). Unlocking the multifaceted molecular functions and diverse disease implications of lactylation. *Biol. Rev. Camb. Philos. Soc*., **100**(1): 172-189.

Kwah JH and Peters AT (2019). Asthma in adults: Principles of treatment. *Allergy Asthma Proc.*, **40**(6): 396-402.

Li D, Shen C, Liu L, Hu J, Qin J, Dai L, Gao L, Cheng M, Wang D, Bao R and Wang B (2022). PKM2 regulates cigarette smoke-induced airway inflammation and epithelial-to-mesenchymal transition via modulating PINK1/Parkin-mediated mitophagy. *Toxicology*, **477**: 153251.

Li H, Lin X, Li C, Li J, Xu X, Meng D and Zheng S (2019). MiR-1286 inhibits lung cancer growth through aerobic glycolysis by targeting PKM2. *Arch. Med. Sci.*, **19**(1): 151-159.

Li M, Li M, Hou Y, He H, Jiang R, Wang C and Sun S (2023). Ferroptosis triggers airway inflammation in asthma. *Ther. Adv. Respir. Dis.*, **17**: 17534666231208628.

Li P, Gu L, Bian Q, Jiao D, Xu Z and Wang L (2021). Long non-coding RNA MALAT1 enhances the protective effect of dexmedetomidine on acute lung injury by sponging miR-135a-5p to downregulate the ratio of X-box binding proteins XBP-1S/XBP-1U. *Bioengineered*, **12**(1): 6377-6389.

Liu K, Liu R, Zhang C, Huang D, Wei B, Song Y, Wang C, Zhang X, Zheng M and Yan G (2025). Suzi Daotan Decoction alleviates asthmatic airway remodeling through the AMPK/SIRT1/PGC-1α signaling pathway and PI3K/AKT signaling pathway. *Sci. Rep.*, **15**(1): 6690.

Liu L, Zhou L, Wang LL, Zheng PD, Zhang FQ, Mao ZY, Zhang HJ and Liu HG (2023). Programmed cell death in asthma: apoptosis, autophagy, pyroptosis, ferroptosis and necroptosis. *J. Inflamm. Res.*, **16**: 2727-2754.

Lizhong D, Qiang Z, Yingying S, Yibu K, Yongfu S and Yongji W (2024). Untargeted serum metabonomic reveals alleviated ovalbumin-induced asthma by Baijin Pingchuan through primary bile acid biosynthesis. *J. Tradit. Chin. Med.Chin. Med.*, **44**(6): 1187-1193.

Lommatzsch M, Brusselle GG, Levy ML, Canonica GW, Pavord ID, Schatz M and Virchow JC (2023). A2BCD: A concise guide for asthma management. *Lancet Respir. Med.*, **11**(6): 573-576.

Melén E, Zar HJ, Siroux V, Shaw D, Saglani S, Koppelman GH, Hartert T, Gern JE, Gaston B, Bush A and Zein J (2024). Asthma inception: Epidemiologic risk factors and natural history across the life course. *Am. J. Respir. Crit. Care Med.*, **210**(6): 737-754.

Nguyen H and Nasir M (2024). Management of chronic asthma in adults. *Med. Clin. North Am.*, **108**(4): 629-640.

Nguyen V, Zhang Q, Pan F, Jin Q, Sun M, Tangthianchaichana J, Du S and Lu Y (2023). Zi-Su-Zi decoction improves airway hyperresponsiveness in cough-variant asthma rat model through PI3K/AKT1/mTOR, JAK2/STAT3 and HIF-1α/NF-κB signaling pathways. *J. Ethnopharmacol.*, **314**: 116637.

Ramsahai JM, Hansbro PM and Wark PAB (2019). Mechanisms and management of asthma exacerbations. *Am. J. Respir. Crit. Care Med.*, **199**(4): 423-432.

Shi C, Li J and Li J (2021). Ephedrine attenuates cerebral ischemia/reperfusion injury in rats through NF-κB signaling pathway. *Hum. Exp. Toxicol.*, **40**(6): 994-1002.

Sun B, Cai F, Yu L, An R, Wei B and Li M (2024). Quercetin inhibits ferroptosis through the SIRT1/Nrf2/HO-1 signaling pathway and alleviates asthma disease. *Transl. Pediatr.*, **13**(10): 1747-1759.

Sun K, Shi Y, Yan C, Wang S, Han L, Li F, Xu X, Wang Y, Sun J, Kang Z and Shi J (2025). Glycolysis-derived lactate induces ACSL4 expression and lactylation to activate ferroptosis during intervertebral disc degeneration. *Adv. Sci.* (Weinh), **12**(21): e2416149.

Tang W, Qin J, Zhou Y, Wang W, Teng F, Liu J, Yi L, Cui J, Zhu X, Wang S, Dong J and Wei Y (2023). Regulation of ferroptosis and ACSL4-15LO1 pathway contributed to the anti-asthma effect of acupuncture. *Int. Immunopharmacol.*, **115**: 109670.

Tian H, Wang L and Fu T (2023). Ephedrine alleviates bleomycin-induced pulmonary fibrosis by inhibiting epithelial-mesenchymal transition and restraining NF-κB signaling. *J. Toxicol. Sci.*, **48**(10): 547-556.

van de Wetering C, Manuel AM, Sharafi M, Aboushousha R, Qian X, Erickson C, MacPherson M, Chan G, Adcock IM, Zounemat-Kermani N, Schleich F, Louis R, Bohrnsen E, D'Alessandro A, Wouters EF, Reynaert NL, Li J, Wolf CR, Henderson CJ, Lundblad LKA, Poynter ME, Dixon AE, Irvin CG, van der Vliet A, van der Velden JL and Janssen-Heininger YM (2021). Glutathione-S-transferase P promotes glycolysis in asthma in association with oxidation of pyruvate kinase M2. *Redox Biol.*, **47**: 102160.

Wang HL, Chen FQ and Wu LJ (2022). Ephedrine ameliorates chronic obstructive pulmonary disease (COPD) through restraining endoplasmic reticulum (ER) stress *in-vitro* and *in-vivo*. *Int. Immunopharmacol.*, **103**: 107842.

Wang Q, Cui Y, Wu X and Wang J (2021). Riparin II potentiates the effect of ephedrine on inflammation and remodelling in the airway of rats suffering from asthma by regulating transforming growth factor-β/Smad3 signalling pathway. *Int. Immunopharmacol.*, **90**: 107116.

Wang W, Yao Q, Teng F, Cui J, Dong J and Wei Y (2021). Active ingredients from Chinese medicine plants as therapeutic strategies for asthma: Overview and challenges. *Biomed. Pharmacother.*, **137**: 111383.

Wang Y, Wan R, Peng W, Zhao X, Bai W and Hu C (2023). Quercetin alleviates ferroptosis accompanied by reducing M1 macrophage polarization during neutrophilic airway inflammation. *Eur. J. Pharmacol.*, **938**: 175407.

Xiang T, Wang X, Huang S, Zhou K, Fei S, Zhou B, Yue K, Li Q, Xue S, Dai Y, Zhang J, Ni H, Sun C and Huang X (2025). Inhibition of PKM2 by shikonin impedes TGF-β1 expression by repressing histone lactylation to alleviate renal fibrosis. *Phytomedicine*, **136**: 156324.

Xiang Y, Jiang Z, Yang Z, Gong S and Niu W (2024). Ephedrine attenuates LPS-induced M1 polarization of alveolar macrophages via the PKM2-mediated glycolysis. *Toxicol. Res.* (Camb), **13**(5): tfae166.

Xie X, Wen C, Peng Q, Xiang D, Pan X, Lan X, Chen Z, Hua X, Wang G and Huang C (2025). H3K9/18 lactylation regulates DNA damage due to nickel exposure in human bronchial epithelial cells. *Toxicol. Appl. Pharmacol.*, **499**: 117347.

Xu M, Zhang D and Yan J (2024). Targeting ferroptosis using Chinese herbal compounds to treat respiratory diseases. *Phytomedicine*, **130**: 155738.

Yang W and Lu Z (2015). Pyruvate kinase M2 at a glance. *J. Cell Sci.*, **128**(9): 1655-1660.

Yasaratne D, Idrose NS and Dharmage SC (2023). Asthma in developing countries in the Asia-Pacific Region (APR). *Respirology*, **28**(11): 992-1004.

Yu H, Zhang C, Pan H, Gao X, Wang X, Xiao W, Yan S, Gao Y, Fu J and Zhou Y (2024). Indeno[1,2,3-cd]pyrene enhances the sensitivity of airway epithelial cells to ferroptosis and aggravates asthma. *Chemosphere,* **363**: 142885.

Yuan JY, Tong ZY, Dong YC, Zhao JY and Shang Y (2022). Research progress on icariin, a traditional Chinese medicine extract, in the treatment of asthma. *Allergol. Immunopathol.* (Madr), **50**(1): 9-16.

Zheng Q, Mu X, Pan S, Luan R and Zhao P (2023). Ephedrae herba: A comprehensive review of its traditional uses, phytochemistry, pharmacology and toxicology. *J. Ethnopharmacol.*, **307**: 116153.

Zhu S, Guo Y, Zhang X, Liu H, Yin M, Chen X and Peng C (2021). Pyruvate kinase M2 (PKM2) in cancer and cancer therapeutics. *Cancer Lett.*, **503**: 240-248.